Supporting Information on

Spectroscopic and theoretical study on the counterion effect of Cu(II) ions and graphene oxide interaction with titanium dioxide

Shujun Yu[a], Xiangxue Wang[a], Yuejie Ai[a,b*], Yu Liang[a], Yongfei Ji[b], Jiaxing Li[a,c], Tasawar Hayat[c,d], Ahmed Alsaedi[c], and Xiangke Wang[a,c,e*]

a. School of Environment and Chemical Engineering, North China Electric Power University, Beijing 102206, P. R. China.

b. Theoretical Chemistry and Biology, School of Biotechnology, Royal Institute of Technology, Roslagstullsbacken 15, 10691 Stockholm, Sweden.

c. NAAM Research Group, Faculty of Science, King Abdulaziz University, Jeddah 21589, Saudi Arabia

d. Department of Mathematics, Quaid-I-Azam University, Islamabad 44000, Pakistan

e. Collaborative Innovation Center of Radiation Medicine of Jiangsu Higher Education Institutions, School for Radiological and Interdisciplinary Sciences, Soochow University, Suzhou 215123, P.R. China

*: Corresponding authors. xkwang@ncepu.edu.cn (X.K. Wang), Tel(Fax): +86-10-61772890. aiyuejie314@126.com (Y.J. Ai).

Synthesis of graphene oxide (GO). The GO was synthesized by chemical oxidation of expanded graphite using modified Hummers method.[1] Typically, 2.0 g of flake graphite (48 μm, 99.95% purity) and 1.5 g $NaNO_3$ (as co-solvent) were added into 250 mL round bottom flask, then 150 mL concentrated H_2SO_4 was added under stirring and ice-water bath conditions. Then 9.0 g of the oxidizing agent ($KMnO_4$) was slowly added into the suspension more than 2 h, the suspension was continually stirred for 5 d at room temperature. Then 280 mL of 5 wt % H_2SO_4 was added and the temperature was kept at 98 °C for 2 h. 12 mL of H_2O_2 (30 wt %) was added in the suspension when the temperature was reduced to 60 °C. After reactions, the mixture was centrifuged and washed with 10 wt % H_2SO_4 solution to remove residual metal ions. The precipitate was then washed with distilled water and centrifuged repeatedly until the solution became neutral. The GO was obtained by centrifuging at 18000 rpm for 60 min after ultrasonic treatment at 400 W for 30 min.

Characterization. The TiO_2 was further characterized by using X-ray diffraction (XRD) and size distribution. The GO was characterized by using transmission electron microscopy (TEM), Fourier-transform infrared spectroscopy (FTIR), X-ray photoelectron spectroscopy (XPS), Raman spectroscopy and size distribution. The XRD pattern was recorded on a MAC Science Co. M18XHF diffractometer by using CuKα radiation (λ = 0.154 nm). The TEM image was obtained by a transmission electron microscope (JEM-1011, Japan). FTIR spectrum was performed by a Bruker

Tensor 27 FTIR spectrophotometer in the range of 4000 - 400 cm^{-1} using the KBr disc technique. XPS data was acquired with a Thermo Escalab 250 XPS with Al Kα radiation at 150 W. Raman spectroscopy was carried out on the InVia Reflex Raman spectrometer (Renishaw) at 532 nm.

The characterization results of TEM, FTIR, XPS and Raman of the prepared GO are given in Figure S2. The TEM image (Figure S2A) shows that GO nanosheets are closely agglomerated together by thin and randomly aggregated nanosheets. According to the FTIR spectrum (Figure S2B), the characteristic bands at 1060 cm^{-1} (C-O bond), 1228 cm^{-1} (C-O-C bond), 1400 cm^{-1} (C-OH vibration), 1622 cm^{-1} (stretching of benzene ring) and 1728 cm^{-1} (C=O stretching vibration) are found, which indicates that large amounts of oxygen-containing functional groups (hydroxyl, carboxyl, carbonyl and epoxy groups) are present on the surface of GO.[2] The degree of oxidation with different functional groups is further demonstrated by XPS. The C1s XPS spectrum of GO (Figure S2C) shows a dominant peak of sp^2 C=C at 284.7 eV, which is attributed to the graphitic structure. Several small peaks of C-O at 286.1 eV and C=O at 288.7 eV are assigned to carbon atoms attached to different oxygen-containing moieties.[3,4] Furthermore, the ratio of C-C/C-O/C=O calculated from the ratio of C-C/C-O/C=O XPS peak area is 10 : 3 : 1. The main features in the Raman spectrum are the so-called “G” and “D” peaks, which lie at around 1580 and 1350 cm^{-1}, respectively, for visible excitation (Figure S2D). The “G” peak is assigned to the bond stretching mode for all pairs of sp^2 atoms in both rings and chains. The “D” peak

is from the vibration of sp^3 carbon atoms of defects and disorder. The weak and broad 2D peak at ~ 2700 cm^{-1} is another indication of disorder as the result of an out-of-plane vibration mode.[4,5] The size diameter distribution of GO under different pH is shown in Figure S3. As the pH decreases from 3.0 to 1.0, the size diameter increases from 240 to 6700 nm, indicating large aggregation is formed which is consistent with the findings in the literatures.[6,7]

In the XRD pattern of TiO_2 (Figure S4A), the peaks at 25.4°, 37.7°, 48.1°, 53.9°, 55.1° and 62.6° are indexed to the typical representations of the anatase phase of (101), (004), (200), (105), (211) and (204) reflections (JCPDS card No. 21-1272), respectively.[8] The size diameter distribution of TiO_2 under different pH is shown in Figure S4B. The size of the TiO_2 is approximately 90 nm at the whole pH, indicating that TiO_2 is chemically stable in aquatic solution.

Computational Details.

The graphene model is built by the unit cell parameters of graphite: $a = b = 2.460$ Å, $c = 6.800$ Å; $\alpha = \beta = 90°$, $\gamma = 120°$ (Figure S5A). For the TiO_2, since the peaks in the XRD patterns of TiO_2 (Figure S4A) are well indexed to the structure of anatase (JCPDS card NO. 21-1272), we took the unit cell parameters of the anatase TiO_2 as $a = b = 3.776$ Å, $c = 9.486$ Å; $\alpha = \beta = \gamma = 90°$ (Figure S5B). A four-layer slab is used with the atoms in the bottom two layers are fixed to their bulk positions with a vacuum layer of 2.5 nm. In order to model the interaction between the GO and the TiO_2 surface, a rectangular supercell of graphene ($a' = 5b - 5a$, $b' = 3a + 3b$) is built

to fit the 2 × 2 supercell of TiO_2 (101) surface, and the final lattice parameters of the graphene supercell are *a*' = 21.304 Å, *b*' = 7.38 Å. The GO is constructed randomly by oxygen atoms at the bridge site with a C : O ratio of 5 : 1. The optimized structures of GO and TiO_2 are shown in Figure S6A and S6B, respectively.

Sorption Isotherms. The sorption isotherms of GO and Cu(II) on TiO_2 at 293, 308 and 323 K are shown in Figure S7. The highest sorption isotherm is found at 323K and the lowest isotherm is found at 293K, suggesting that higher temperature is more conducive to GO and Cu(II) sorption on TiO_2. To quantify the sorption data and to gain a better understanding of the sorption mechanism, the Langmuir and Freundlich models are applied to simulate the experimental data. The Langmuir isotherm model usually describes the monolayer sorption process that takes place on a homogeneous surface.[9] It can be expressed by the following equation:

$$q_e = \frac{bq_{\max}C_e}{1+bC_e} \tag{1}$$

where $q_{\max}$ (mg/g) is the maximum sorption capacity, *b* (L/mol) is a binding constant that relates to the heat of sorption. The Freundlich expression is an exponential equation that represents properly the sorption data at low and intermediate concentrations on heterogeneous surfaces.[10] Its form can be expressed as:

$$q_e = K_F C_e^n \tag{2}$$

where K_F (mg^{1-n} L^n/g) represents the sorption capacity when the equilibrium concentration of GO and Cu(II) equals to 1, and *n* represents the degree of dependence of sorption with equilibrium concentration. As shown in Table S1, GO

and Cu(II) sorption on TiO_2 can be satisfactorily fitted by Langmuir model ($R^2 > 0.9$) as compared to Freundlich model ($R^2 < 0.9$), indicating the monolayer sorption of GO and Cu(II) on TiO_2. The maximum sorption capacities (q_{max}) of GO and Cu(II) on TiO_2 calculated from Langmuir model are 60.0 and 32.3 mg/g at 293 K, respectively (Table S1). Furthermore, the sorption isotherm of Cu(II) on GO at 293 K is shown in Figure 1G and the q_{max} value of Cu(II) on GO is calculated to be 45.2 mg/g. Comparing the sorption properties of Cu(II) on different materials (Table S3), one can see that the GO has higher sorption capacity due to its abundant functional groups such as hydroxyl, carboxyl and epoxy groups (Figure S2), which can form strong surface complexes with heavy metal ions.[4,11,12] Thus, when Cu(II) coexist with GO in the aqueous solutions, they may influence each other.

The amounts of GO retained by TiO_2 for different addition sequences are shown in Figure 1E. The q_{max} values of GO adsorbed on TiO_2 are in the order of (TiO_2-GO)-Cu > (GO-Cu)-TiO_2 > (TiO_2-Cu)-GO > TiO_2-GO. In the system of (TiO_2-Cu)-GO, the sorption of Cu(II) to TiO_2 particles increases the TiO_2 surface charge and enhances the sorption of negatively charged GO molecular to TiO_2-Cu. Therefore, the q_{max} value of GO in (TiO_2-Cu)-GO system is higher than TiO_2-GO system. But, the surface-bound Cu(II) may block parts of active sites on TiO_2 surface and prevents GO from reaching them when added later due to the steric effects, hindering GO uptake. Although the firstly adsorbed Cu(II) ions occupy some sorption sites on GO, many oxygen containing groups on GO can still interact with terminal -OH on TiO_2 through

hydrogen bond. In addition, the GO in aqueous solutions can also interact with the unoccupied surface functional groups of TiO_2 and further improves the removal of GO, so the sorption capacity of GO in (GO-Cu)-TiO_2 system is higher than (TiO_2-Cu)-GO system. TiO_2 has stronger complexation ability with GO through electrostatic attraction and hydrogen bond than Cu(II) and the pre-adsorbed Cu(II) can lower the negative surface charge of GO, so the removal of GO is in the order of (TiO_2-GO)-Cu > (GO-Cu)-TiO_2.

From the sorption isotherms of Cu(II) on coexisting TiO_2 systems at different addition sequences (Figure 1F), the q_{max} values of Cu(II) are calculated to be 56.0 mg/g for (TiO_2-GO)-Cu, 45.1 mg/g for (GO-Cu)-TiO_2, 42.8 for (TiO_2-Cu)-GO and 32.3 mg/g for TiO_2-Cu. In (TiO_2-Cu)-GO system, the Cu(II) ions are firstly adsorbed on TiO_2 through surface complexation, then the TiO_2-Cu complexes interact with GO through electrostatic attraction and hydrogen bond, and the remaining Cu(II) in the aqueous solutions can also interact with the oxygen-containing functional groups of GO. So, the q_{max} value of Cu(II) in (TiO_2-Cu)-GO system is higher than single-adsorbate system. The sorption of Cu(II) in (GO-Cu)-TiO_2 system is similar to that of (TiO_2-Cu)-GO system. But due to its negatively charged surface and abundant oxygen-containing functional groups (e.g. OH and COO^-), GO can interact with more Cu(II) ions by electrostatic attraction and surface complexation as compared with TiO_2. Therefore, the q_{max} value of Cu(II) on (GO-Cu)-TiO_2 is slightly higher than that of Cu(II) on (TiO_2-Cu)-GO. In the system of (TiO_2-GO)-Cu, the sorption of GO

molecules to TiO_2 particles decreases the TiO_2 surface charge and enhances the sorption of positively charged Cu(II) ions to TiO_2-GO. The surface adsorbed GO can also provide more functional groups and available sites to bind Cu(II) ions through the formation of surface complexes, and thereby results in more Cu(II) ions' sorption. The results indicate that GO plays an important role in the enhanced retention of Cu(II) on TiO_2 through the formation of strong surface complexes.

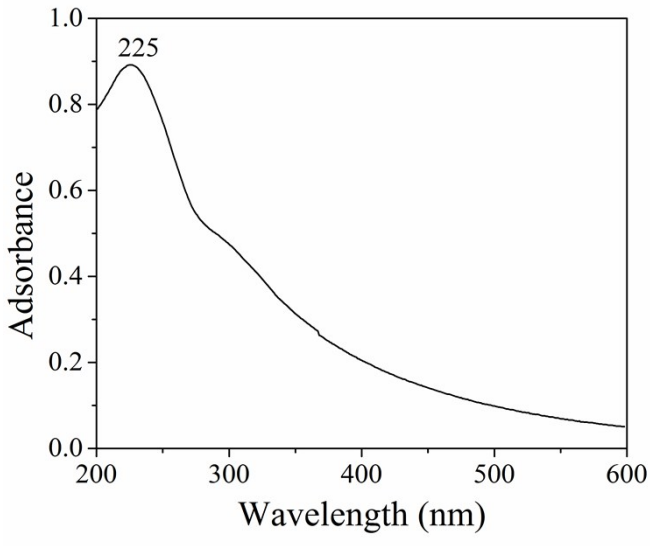

Figure S1. The UV-vis absorption curve of GO.

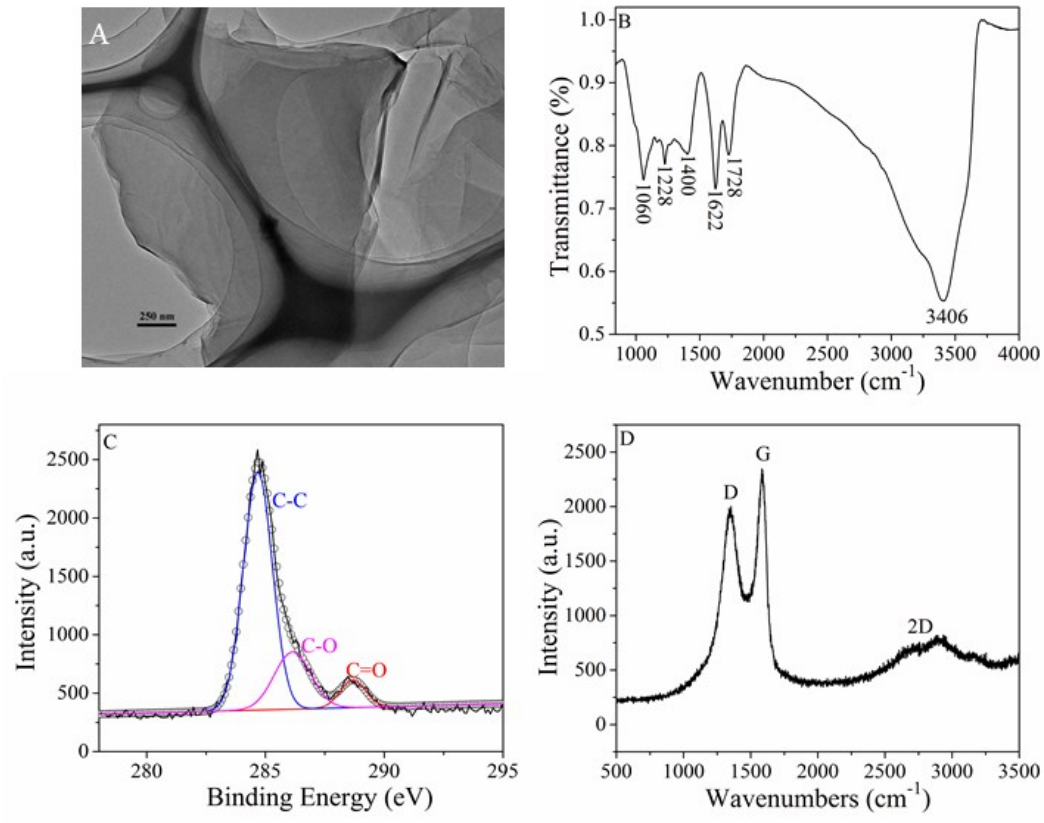

Figure S2. The characterization of GO: (A) TEM image; (B) FTIR spectrum; (C) C 1s XPS survey spectrum and (D) Raman spectrum.

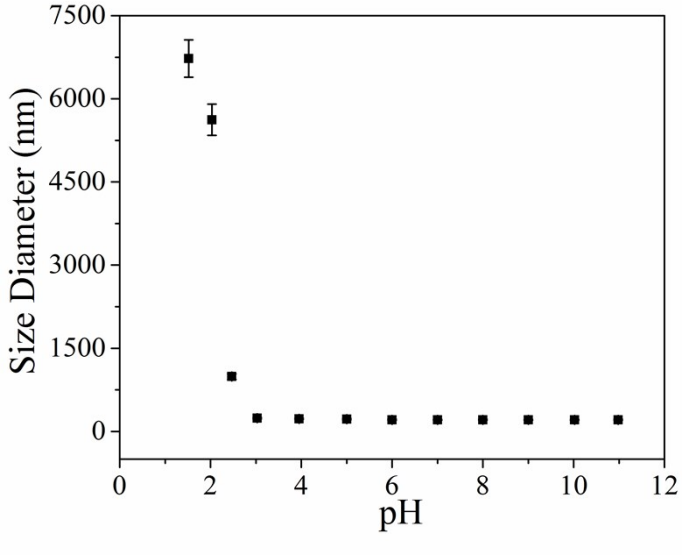

Figure S3. Size diameter under different pH values.

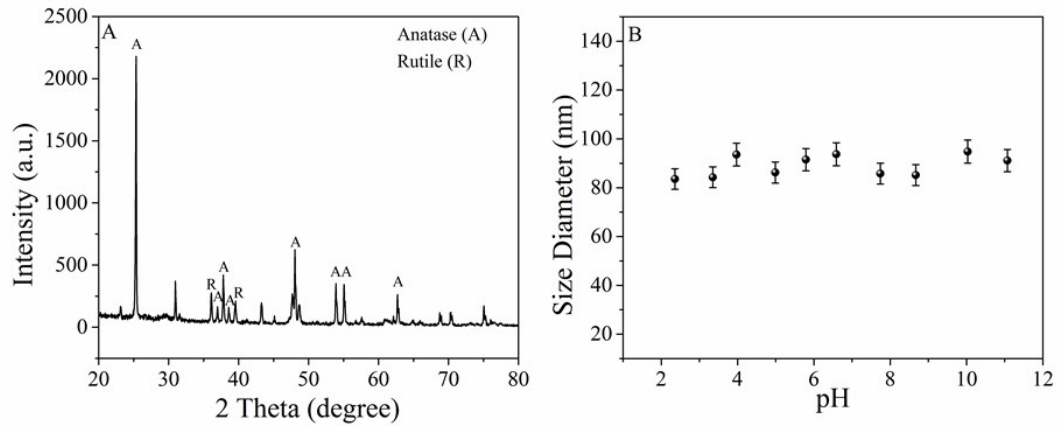

Figure S4. The characterization of TiO_2: (A) XRD pattern; (B) Size diameter under different pH values.

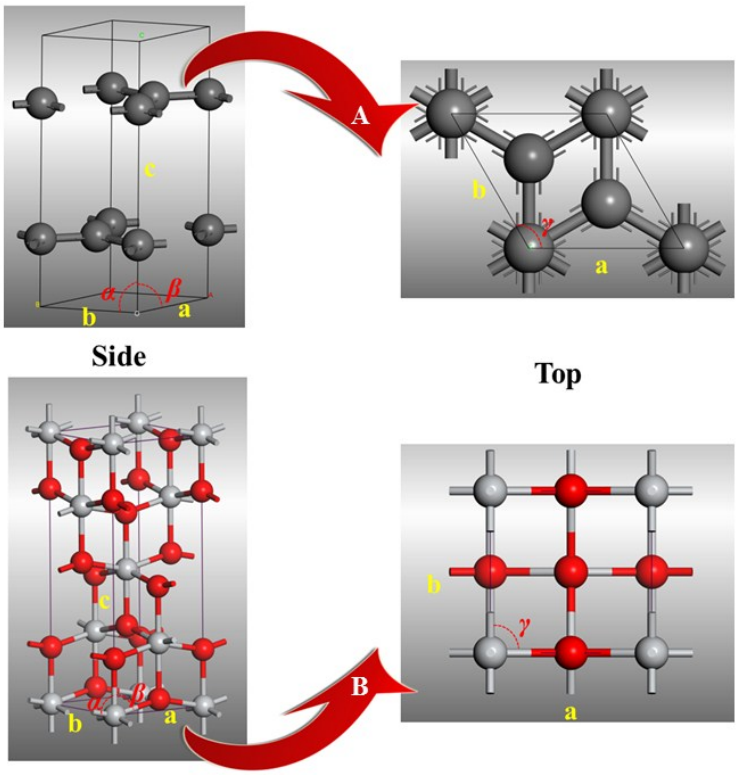

Figure S5. The unit cell parameters of the GO (A) and TiO_2 (B).

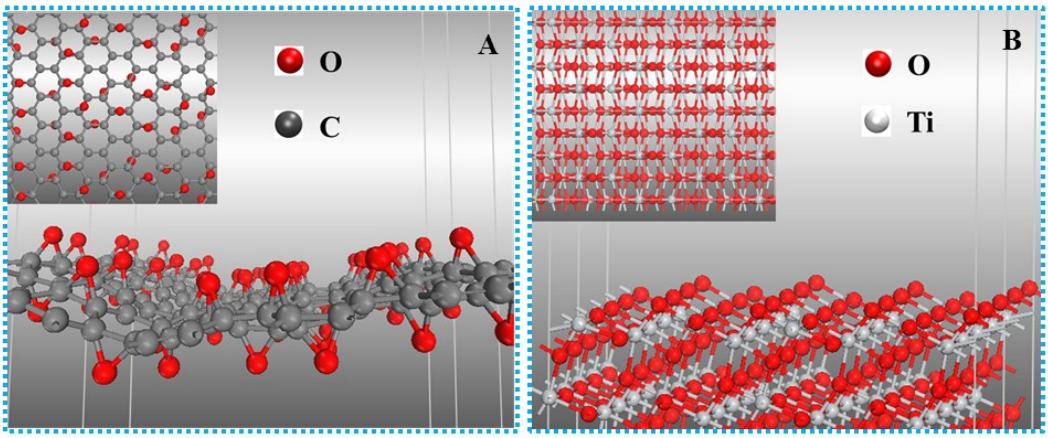

Figure S6. The optimized structures for GO (A) and TiO_2 (B) from the top view and side view.

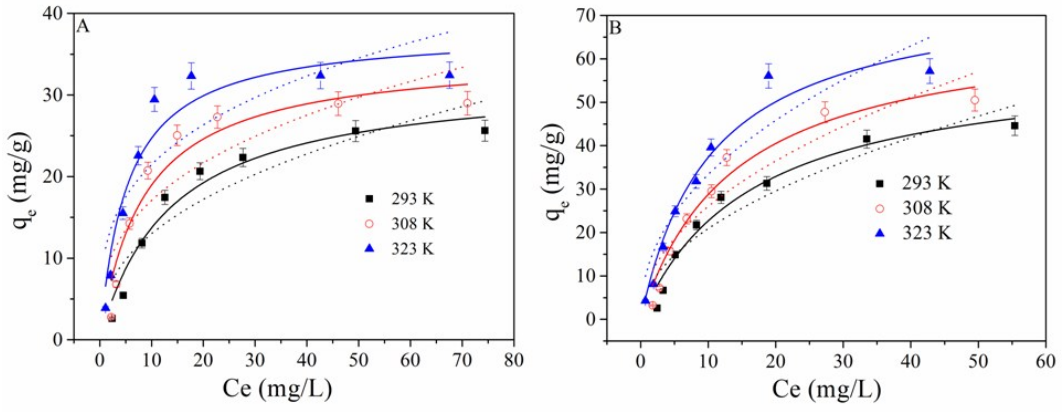

Figure S7. Sorption isotherms of Cu(II) (A) and GO (B) on TiO_2. pH = 5.0 ± 0.1, I = 0.01 mol/L $NaNO_3$, m/V = 1 g/L. The solid lines represent the Langmuir model. The dashed lines represent the Freundlich model.

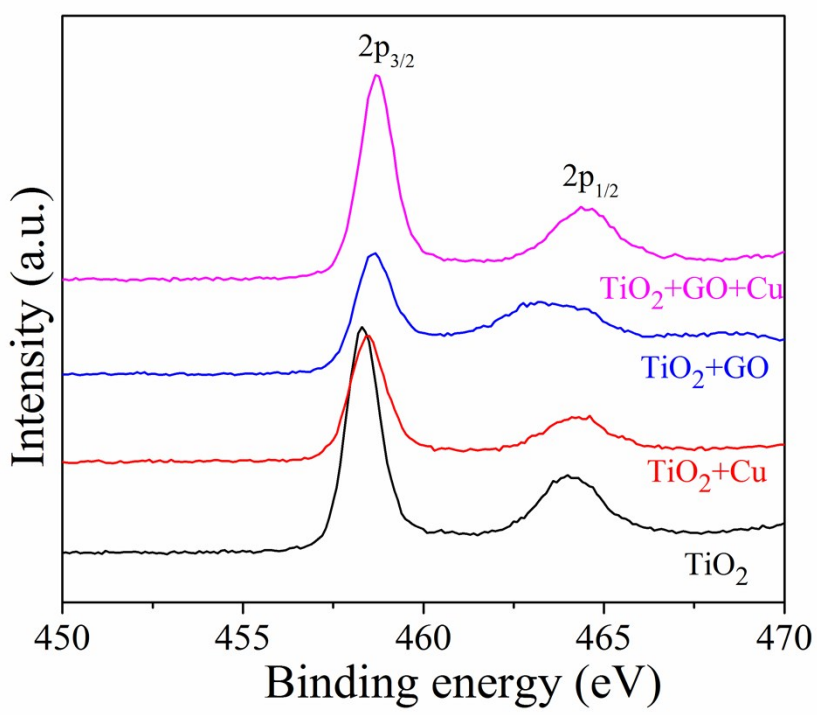

Figure S8. Ti 2p XPS spectra of TiO_2, TiO_2+Cu, TiO_2+GO and TiO_2+GO+Cu.

Table S1. Parameters for the Langmuir and Freundlich isotherm models at different temperatures.

Adsorbate	T (K)	Langmuir model			Freundlich model		
		q_{max} (mg/g)	b (L/mol)	R^2	K_F (mg^{1-n} L^n/g)	n	R^2
Cu(II)	293	32.3	0.07	0.954	5.1	0.41	0.825
	308	35.1	0.12	0.920	7.7	0.34	0.738
	323	37.9	0.19	0.932	10.9	0.30	0.716
GO	293	60.0	0.06	0.961	6.6	0.50	0.884
	308	68.5	0.07	0.960	8.5	0.49	0.865
	323	76.3	0.10	0.965	11.6	0.46	0.868

Table S2. Binding energies (E_b) of elements in TiO_2 before and after removal of Cu(II) and GO.

Sample	E_b (eV)			
	Ti2p	O1s	C1s	Cu2p
TiO_2	457.47	531.96	--	--
TiO_2+Cu	459.54	534.28	--	935.05
TiO_2+GO	463.66	535.12	293.04	--

TiO_2+GO+Cu	465.98	536.34	284.54	937.37

Table S3. Comparison of Cu(II) sorption capacities on different adsorbents.

Adsorbents	Experimental conditions			q_{max} (mg/g)	References
	pH	T (K)	m/V (g/L)		
TEPA modified carbon sphere	5.0	-	10	33.33	[13]
LDH-Cl	5.0	298	1.7	38.77	[14]
montmorillonite	5.0	-	5	14.87	[15]
Fe_3O_4	5.3	293	0.4	11.89	[11]
GO/Fe_3O_4	5.3	293	0.4	18.26	
TiO_2	5.0	293	0.1	32.3	This study
GO	5.0	293	0.05	45.2	

References

(1) W. S. Hummers and R. E. Offeman, *J. Am. Chem. Soc.* 1958, **80**, 1339.

(2) Y. B. Sun, Q. Wang, C. L. Chen, X. L. Tan and X. K. Wang, *Environ. Sci. Technol.* 2012, **46**, 6020-6027.

(3) S. J. Yu, X. X. Wang, Y. J. Ai, X. L. Tan, T. Hayat, W. P. Hu and X. K. Wang, *J. Mater. Chem. A* 2016, **4**, 5654-5662.

(4) G. X. Zhao, J. X. Li, X. M. Ren, C. L. Chen and X. K. Wang, *Environ. Sci. Technol.* 2011, **45**, 10454-10462.

(5) S. J. Yu, Q. Wei, B. Du, D. Wu, H. Li, L. G. Yan, H. M. Ma, and Y. Zhang, *Biosens. Bioelectron.* 2013, **48**, 224-229.

(6) L. Wu, L. Liu, B. Gao, R. Munoz-Carpena, M. Zhang, H. Chen, Z. Zhou and H. Wang, *Langmuir* 2013, **29**, 15174-15181.

(7) I. Chowdhury, M. C. Duch, N. D. Mansukhani, M. C. Hersam and D. Bouchard, *Environ. Sci. Technol.* 2013, **47**, 6288-6296.

(8) Y. Liang, H. Wang, H. Sanchez Casalongue, Z. Chen and H. Dai, *Nano Res.* 2010, **3**, 701-705.

(9) I. Langmuir, *J. Am. Chem. Soc.* 1918, **40**, 1361-1403.

(10) H. Freundlich, *J. Phys. Chem.* 1906, **57**, 385-470.

(11) J. Li, S. Zhang, C. Chen, G. Zhao, X. Yang, J. Li, X. Wang, *ACS Appl. Mater. Inter.* 2012, **4**, 4991-5000.

(12) S. Yu, X. Wang, X. Tan and X. Wang, *Inorg. Chem. Front.* 2015, **2**, 593-612.

(13) W. Peng, Z. Xie, G. Cheng, L. Shi and Y. Zhang, *J. Hazard. Mater.* 2015, **294**, 9-16.

(14) M. A. González, I. Pavlovic and C. Barriga, *Chem. Eng. J.* 2015, **269**, 221-228.

(15) L. Ma, Q. Chen, J. Zhu, Y. Xi, H. He, R. Zhu, Q. Tao and G. A. Ayoko, *Chem. Eng. J.* 2016, **283**, 880-888.